

CHAPTER 168

IMPULSIVE BREAKING WAVE FORCES ON AN INCLINED PILE EXERTED BY RANDOM WAVES

by

K. TANIMOTO*, S. TAKAHASHI*, T. KANEKO**, K. SHIOTA**

ABSTRACT

A calculation method of the impulsive breaking wave forces on piles is proposed in this paper. It is derived on the basis of experimental results with some theoretical considerations. Wave forces on a cylinder caused by both regular and irregular trains of waves are measured in a large wave flume. The experimental results are compared with the values predicted by both Wagner and Karman. In the proposed method, it is assumed that the impulsive force acts on the upper half of the pile between the still water level and the wave crest, and that the force distribution along the pile is triangular shape. The peak value in the distribution is expressed by the function of both the breaking force parameter and the inclination angle of the cylinder. The breaking force parameter is the ratio of the bottom slope to wave steepness. The time history of the impact force is given as a triangular pulse with a vertical rise. The duration time is determined as half of the value predicted by Karman's theory.

1. INTRODUCTION

Wave forces which act on cylindrical members supporting coastal and offshore structures are generally predicted as the sum of drag and inertia forces. However, impact forces should be counted in addition to these forces when breaking waves act on a pile.

A prediction method for the impact force is shown in the Shore Protection Manual(1975) on the basis of the experimental studies by Ross(1955,1959) and Hall(1958). According to the method, the total force by a breaking wave can be estimated by Morison's equation with the drag coefficient being 2.5 times the ordinary value. The experiments by Ross and Hall, however, were conducted with a steep bottom slope condition. The impact force is very large if the bottom slope is steep. The value of the impact force estimated by the formula, therefore, may be excessive for a gentle bottom slope condition. The dynamic response of structures resisting such an impact

* Hydraulic Engineering Division, Port and Harbour Research Institute
Ministry of Transport, 3-1-1 Nagase, Yokosuka, Japan

** Engineering and Construction Division, Kawasaki Steel Corporation
2-2-3 Uchisaiwai-cho, Chiyoda-ku, Tokyo, Japan

force cannot be predicted, because it provides information only on the peak value of the impact force.

Godá et al. (1966) proposed a calculation method for the impact forces acting on a vertical pile, referring to the virtual fluid mass theory derived by Von Karman(1929). They obtained a diagram for the curling factor, which can evaluate the impact forces for both 1/10 and 1/100 bottom slope conditions. The time history of the impact force can be also predicted by the method.

Many inclined piles are used as the members of sea structures such as sea-berths and jetties. The authors (1986A,B) carried out a series of experiments to investigate the breaking wave force on an inclined pile and proposed a calculation method. The method was an extension of Godá's method.

All of these studies, however, were based on the experiments only by regular waves. Because ocean waves are random, it is important to investigate the wave force exerted by irregular waves. Only Ochi et al. (1984) discussed the statistical characteristics of impact pressure on a pile by random waves.

This paper proposes a calculation method for the impact forces of breaking waves due to random ocean waves. First, some theoretical consideration based on Wagner's theory was given to the impact force which occurs by a collision between the pile and the water surface. Secondly, experiments were conducted to measure the impact forces on the pile due to not only regular waves but also irregular waves. Then, the calculation method was derived. The present method provides information on the impact force including the peak value, the time history, and the distribution along the pile. The method is applicable not only to vertical piles but also to inclined piles.

2. THEORETICAL CONSIDERATION

Wagner (1932) derived a set of equations for the impact pressure due to collision between a rigid body and water surface. Figure 1 shows Wagner's model when the water surface strikes a pile. The water surface "pile-up" along the pile surface can be seen in the figure, which is taken into account in the theory. In this figure, D , R and V are the pile diameter, the pile radius, the uprising velocity of the water surface. An equivalent plate of the width $2b$ is considered between the two attaching points of the pile surface to the water surface. The axis x is parallel to the plate and the axis y is perpendicular to it. Equations which

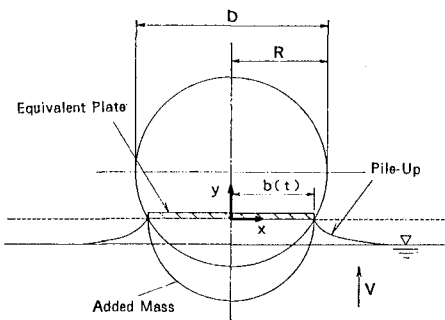


Fig.1 Wagner's model for impact force

determine the water surface profile at time t and the pressure on the pile surface are obtained from the complex potential of the flow around the flat plate.

In the actual calculation of the impact pressure, the pile surface should be expressed as a function of x . Here, the pile surface is approximated by the following equation:

$$\frac{y_1}{R} = \left(\frac{x}{R} \right)^m \quad (1)$$

where, y_1 is the distance of the water surface from the bottom of the pile. Figure 2 shows the approximated profile of pile surface for several values of the power m in Eq.(1). The broken line, the dot-dash line, the two dots-dash line and the dotted line indicate the cases for $m = 1, 2, 3$ and 4 respectively. In the case where $m=1$, the profile by Eq.(1) is actually a wedge with the angle of 45° degrees. The bottom portion of the approximated profile swells as m increases. The profiles for $m = 3$ and 4 are close to a circle which is drawn by the solid line.

Figure 3 shows the time history of the total impact forces on the pile which are obtained from Wagner's theory. The vertical axis is the non-dimensional force $F/(w_0 DV^2/2g)$, where F is the impact force, w_0 is the unit weight of water, and g is the gravity acceleration. The horizontal axis is the nondimensional time $t/(R/V)$. The lines in the figure correspond to the same number of the power m respectively as in Fig.2. The solid line which represents the force on the circular pile based on the Karman's theory is also shown for comparison. Karman's theory neglects the pile-up effect. The followings can be pointed out from the figure:

a) The characteristics of the impact forces change greatly by the change of the pile profile. In the case of the wedge-shape pile ($m = 1$), the force increases linearly with time. When the pile profile

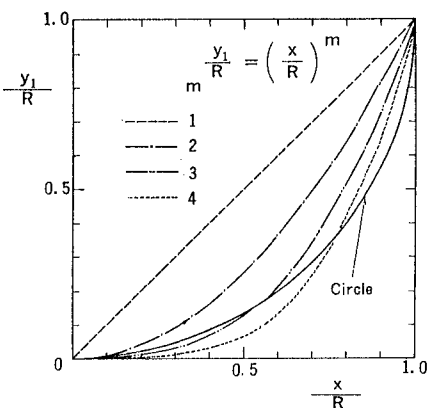


Fig.2 Approximated pile profiles

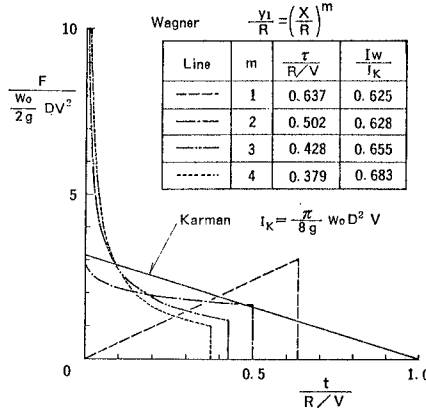


Fig.3 Calculated Impact force

approaches the circular shape ($m = 3$ and 4), the impact force becomes hyperbolic shape with a steep rise at the instant of collision and a sudden decrease after the peak.

- b) The impact force on a circular pile by Wagner's theory is quite different from that by Karman's theory. For example, the peak value when $m=3$ is 471, which is more than one hundred times the peak value by Karman's theory. This is caused by the fact that the incremental rate of added mass of the equivalent flat plate by Wagner's theory is large because of the pile-up phenomenon, which is not considered in Karman's theory. In the range of $t/(R/V) > 0.09$, however, Wagner's impact force is smaller than Karman's one. This is due to the effect of negative pressure induced by the current along the pile surface. This effect is considered only in Wagner's equations.
- c) By the effect of the pile-up, the impact duration time τ by Wagner's theory is shorter than that by Karman's theory. The Wagner's duration time with $m = 3$ is 0.428 times Karman's one.
- d) The impulse of total force by the Wagner's theory is 0.6 - 0.7 times that by Karman's theory. This is also caused by the negative pressure component.

3. EXPERIMENTAL FACILITY AND PROCEDURE

Wave Tank and the Bottom Slope

The experiments were carried out in a large wave tank, which is 105 m long, 3 m wide and 2.5 m deep. The wave tank was divided into 80 and 205 cm wide flumes by a partition wall which was installed 42 m away from the wave generator. The model pile was installed in the 80 cm flume. The piston type wave generator in the wave tank could generate both regular and irregular waves.

The cross sections of the wave flume in the experiments are shown in Fig. 4 (a) and (b). The bottom slope i near the model was fixed at $1/30$ or $1/100$ as shown in the figure. The model pile was installed 72 m away from the wave generator. The water depth at the pile location h is maintained at 70 cm.

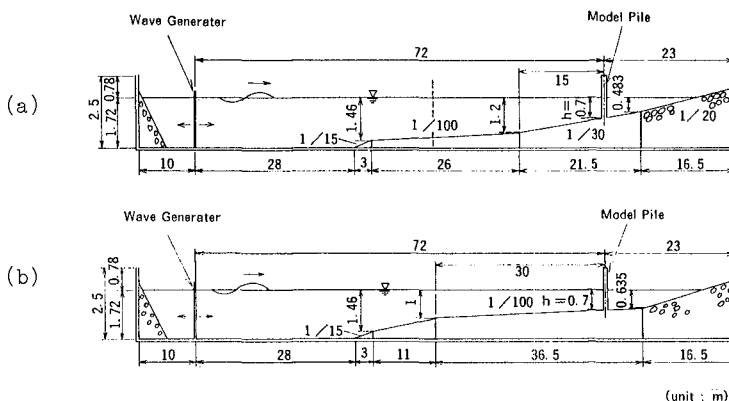


Fig.4 Cross sections of the wave tank

Model Pile and Wave Force Sensors

Figure 5 shows the model pile. The pile inclination was changed at angles $\theta = 0^\circ, \pm 15^\circ$ and $\pm 30^\circ$. The bottom end of the pile was fixed on a base plate. The top end was also fixed to the side wall of the wave tank with a steel beam. The pile diameter D was 14 cm. The model pile comprised thirteen wave force sensors (F1-F13) and two dummy pipes.

The details of the wave force sensor are shown in Fig.6. The sensor was an aluminum pipe with 5 mm thickness and 14 mm diameter, which was connected to a rigid steel pillar by 3 mm thick steel plates. When the wave force acted on the pile, the bending strain appeared in the steel plates. The force component perpendicular to the plates was measured with four strain gauges pasted on the plates. The sensitivity of the sensor was $8.7 \mu / \text{Kgf}$ and the natural frequency was 745 Hz in air and 422 Hz in water. The damping factor was 0.026 in air and 0.068 in water.

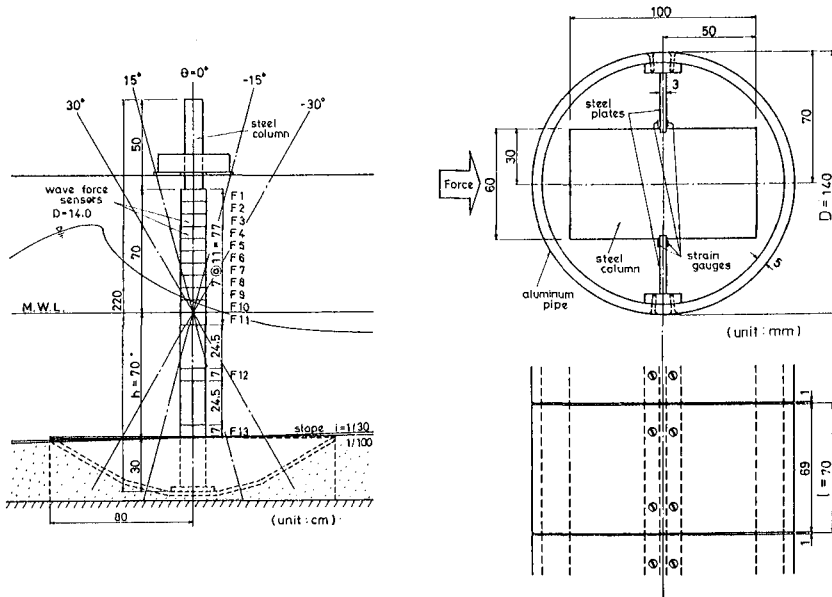


Fig.5 Model pile

Fig.6 Wave force Sensors

Measurement and Analysis Method

The analogue signal from the wave force sensors was sent to a computer through amplifiers and low-pass filters, and was analysed by the computer. The low-pass filters were used not only to cut off the noise but also to reproduce the correct input force signal eliminating the response effect of the sensors. Although the natural frequency of

the sensors was very high, a dynamic response appeared in the sensors when the impact force is very large. The authors (1983) already investigated a method to obtain the impact force signal from the response data. This method was used in the present experiments. The applicability of the method was examined in the preliminary test. The cut-off frequency was set at 400 Hz for the sensors F1 - F10, which were installed above the still water level. For the sensors F11 - F13 which were below the still water level, the cut-off frequency was set at 20 Hz since the impact force did not act on them. The sampling time in the analogue-digital conversion in the computer was 0.005 s.

4. CHARACTERISTICS OF WAVES

Regular Waves

The wave period T of regular waves was set at 2, 3 and 4 s. The wave height was fixed at $H'/H_b = 0.5, 0.8, 0.9, 1.0, 1.1, 1.2$ and 1.7, and the additional values of the wave height were selected near the breaking wave height H_b to obtain the maximum breaking wave force. The term H' is called here "the hypothetical passing wave height", which is the wave height at the measuring point for non-breaking waves but is the breaking wave height at the breaking point for breaking waves. The breaking wave height and the crest elevation η_b were measured in the experiments, which had the values very close to those evaluated by Goda's breaker indices (Goda 1970). The breaking wave velocity C_b measured by 16 mm film agrees very well with the value calculated by

$$C_b = \sqrt{g(h + \eta_b)} \quad (2)$$

Irregular Waves

The irregular waves in the experiments have the Bretschneider-Mituyasu spectrum (see Goda(1985) pp. 23-27). Three wave groups were prepared for the irregular wave tests, namely wave-A, wave-B and wave-C. The significant wave period of the three wave groups $T_{1/3}$ were 2, 3 and 4 s respectively. Each wave group has three wave trains;(A1 - A3), (B1 - B3) and (C1 - C3). Each wave train contains about two hundred waves, and therefore each wave group has about six hundred waves. Three different levels of the significant wave height were employed in the experiments as shown in Table 1. A wave train with the highest level of the significant wave height contains a number of breaking waves, while that of the lowest level has few breaking waves. Six more wave trains were prepared for the wave group B to examine the effect of the number of waves.

Table 1 Significant wave height

Wave Group	$H_{1/3}/h$					
	$i = 1/30$			$i = 1/100$		
A	0.307	0.491	0.556	0.311	0.457	0.519
B	0.370	0.601	0.674	0.359	0.539	0.580
C	0.364	0.656	0.766	0.363	0.557	0.623

The relation between the maximum wave height H_{max} and the maximum wave crest height, η_{max} can be expressed as follows from the results of the wave measurement.

$$\eta_{max}/H_{max} = 0.5 + a\sqrt{H_{max}/h} \quad (3)$$

$$\left. \begin{array}{l} a=0.247 \quad : \quad i=1/30 \\ a=0.315 \quad : \quad i=1/100 \end{array} \right\} \quad (4)$$

5. EXPERIMENTAL RESULTS

Results of Regular Wave Tests

Figure 7 shows profiles of breaking waves striking a pile. This figure was made by tracing the film record for the case of $T = 3$ s, $H' = 55.3$ cm, $i = 1/30$, and $\theta = 0^\circ$. The vertical wave front near the crest is hitting very hardly the sensor F4 in the figure.

Figure 8 shows the time history of the force by the same breaking wave in Fig. 7. F_3 through F_7 indicate the force on the sensors F_3 - F_7 respectively. F is the total force which is obtained by integration of the forces on the sensors. The forces are presented in non-dimensional form with unit weight of water, w_0 , the pile diameter D , the water depth h and the height of the sensor l . Large impact forces are observed in F_4 and F_5 . The time histories of the impact forces are similar to that by Wagner's theory shown in Fig. 3. The rising time is about 0.001 s.

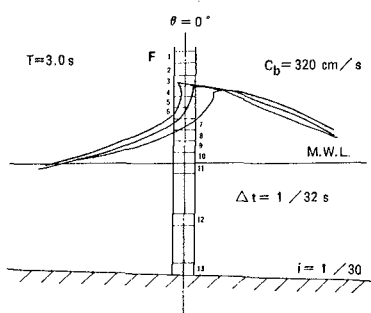


Fig. 7 Profiles of breaking wave striking the pile

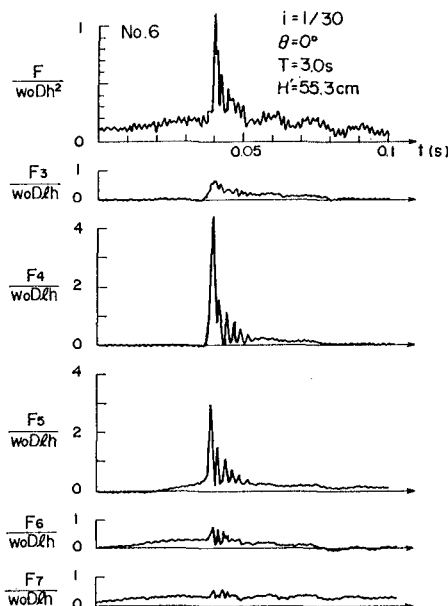


Fig. 8 Time history of impact force by breaking wave

Figure 9 shows the relation between the peak value of the total force F_m and the hypothetical passing wave height H' for the case of $i = 1/30$, $\theta = 0^\circ$ and $T = 3$ s. The arrow in the figure indicates the relative breaking wave height H_b/h . When H' approaches H_b , the impact force acts on the pile, and F_m scatters to a great extent. In the range of $H' > H_b$, the impact force decreases because post-breaking waves acts.

Figure 10 shows the relation between the maximum breaking wave force F and the "breaking force parameter" $i/(H_b/L_0)$, where L_0 is the wave length in deep water. The breaking force parameter represents the change of the breaker type referring to the results of a series of small scale model tests (Authors 1986). The maximum breaking wave force F increases greatly in the range of $i/(H_b/L_0) = 0.4 \sim 0.7$ where the breaker type changes from spilling to plunging. As the pile inclines seaward, the wave which has a straight and sharp front just before breaking whips the face of the pile, causing a large impact force. When the pile inclines shoreward, however, the impact force is reduced. This is because only a small portion of the curling wave front just after breaking hits the face of the pile, and because the other portion of wave front is disturbed by itself.

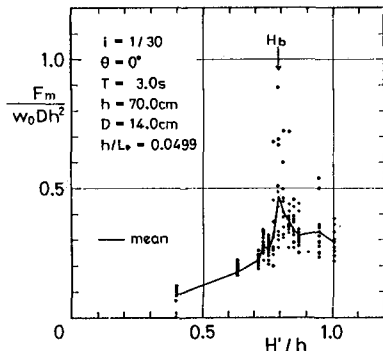


Fig. 9 Wave force vs wave height

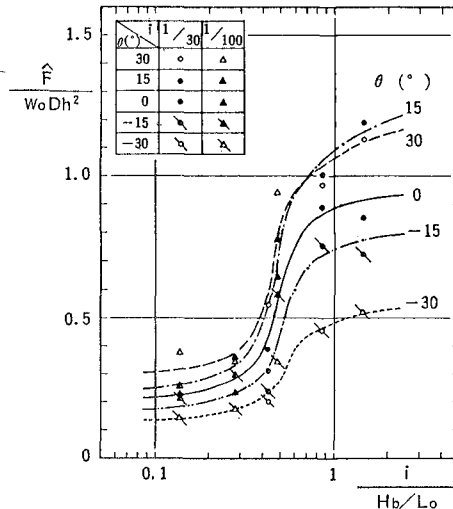


Fig. 10 Maximum impact force

Figure 11 shows the breaking wave force distribution for several values of time when $i = 1/30$, $\theta = 0^\circ$, $T = 4$ s and $H'/h = 0.83$. The vertical axis z is the co-ordinate along the pile from the mean water level. When $t = 0$, a small force acts within the range $z = -60 \sim +20$ cm. When $t = 0.0825$ s, the impact force with a sharp peak is observed just under the crest. The distribution of the impact force is symmetrical and triangular.

Results of Irregular Wave Tests

Figure 12 shows the time history of the water surface elevation

η , the total force F and the force on each wave sensor $F_4 - F_{12}$ for the case of $i = 1/30$, $\theta = 0^\circ$, wave-B(B5), and $H_1/3/h = 0.676$. Large impact forces are observed when the wave profiles are very steep in the figure. The irregularity of the wave forces is much emphasized compared with the irregularity of the waves.

The individual waves for a train of irregular waves are defined by the zero-upcrossing method. The peak values of the total force F_m for the individual waves were statistically analysed and the representative values of the peaks were obtained. The maximum value of

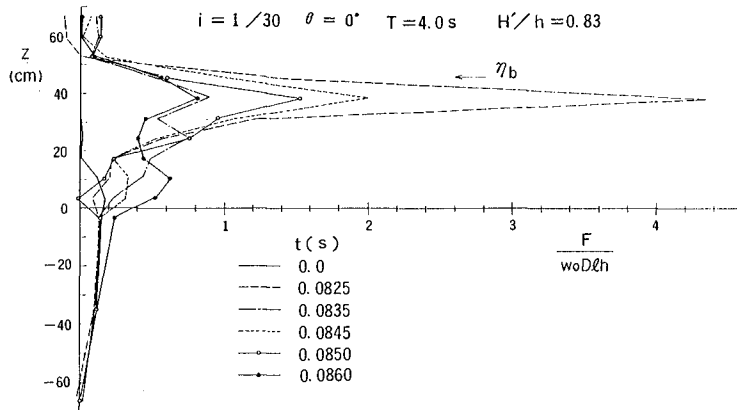


Fig. 11 Distribution of impact force

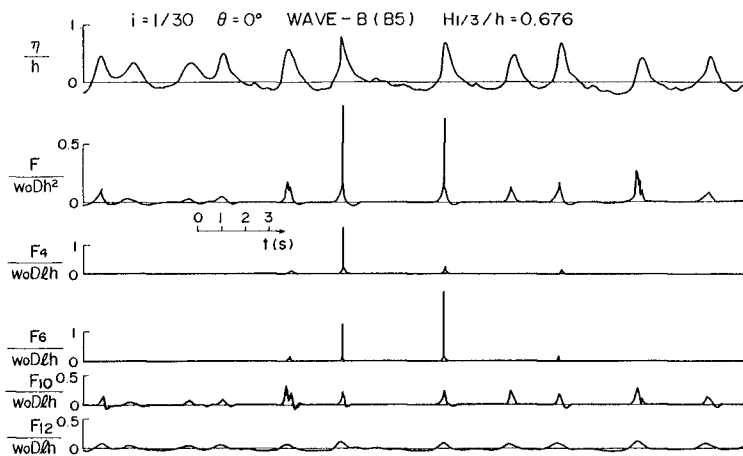


Fig. 12 Wave and wave force profiles by random waves

F_m in a wave train is denoted by F_{max} . The average of F_m from the highest to the 1/10 highest is called the 1/10 largest force $\bar{F}_{1/10}$. The average of F_m from the highest to the 1/3 highest is called the 1/3 largest force $\bar{F}_{1/3}$. The average of all the peak values is denoted by \bar{F}_{mean} respectively. The average of all the representative values for the different wave trains in the same wave group are expressed by \bar{F}_{max} , $\bar{F}_{1/10}$, $\bar{F}_{1/3}$ and \bar{F}_{mean} respectively. The maximum value of F_{max} in a wave group is denoted by F .

Figure 13 (a) and (b) show the frequency distribution of the peak wave force F_m in the form of probability density for the case of $i = 1/30$, $\theta = 0^\circ$ and wave-B(B1-B10). When $H_{1/3}/h = 0.367$ breaking waves were scarcely included, and then maximum value of F_m/F_{mean} is 5.3. When $H_{1/3}/h = 0.676$, a fairly large number of breaking waves were included, and the maximum value of F_m/\bar{F}_{mean} goes up to 7.3. This indicates that the peak values of the impact force vary very widely.

Table 2 shows the mean value and the standard deviation of the maximum force F_{max} to investigate the statistical characteristics of the maximum impact force. This is for the case of $\theta = 0^\circ$ and wave-B. The ratios between the representative forces are also shown. The mean value of F_{max} increases as the increase of $H_{1/3}$. For the case of $H_{1/3} = 0.676$ and $i = 1/30$, the value of \bar{F}_{max} is 0.808 and the standard deviation is 0.172. The columns of B3(Run 1 - 10) show the values when the same wave train B3 was repeated ten times. For the case of $H_{1/3}/h = 0.676$ and $i = 1/30$, the values by the B3 wave train are almost the same as the values by the wave trains from B1 to B10.

Figure 14 shows the relation between the maximum force \hat{F} and the breaking force parameter $i/(H_{max}/L_0)$. The maximum wave height instead

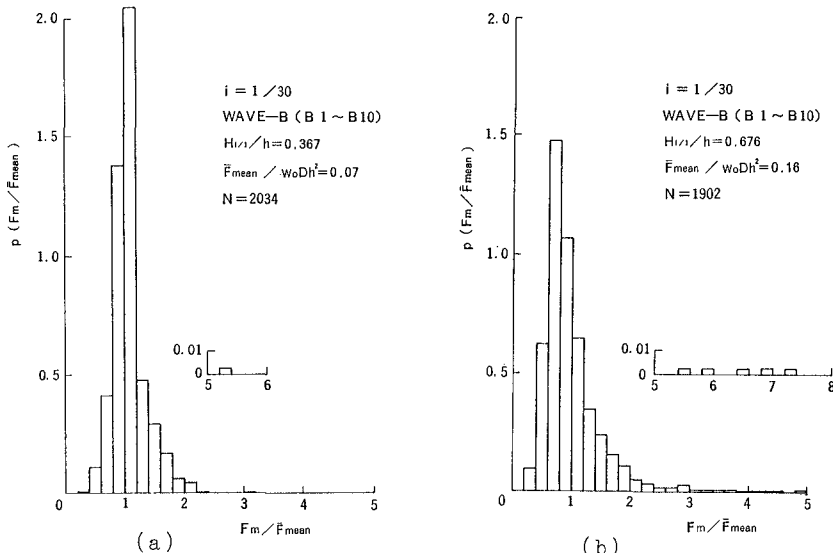


Fig. 13 Frequency of wave forces

Table 2 Statistical characteristics of wave forces

i	wave trains	$H_{1/3}/h$	$F_{max}/w_0 D h^2$			\bar{F}_{max} $\bar{F}_{1/3}$	$\bar{F}_{1/10}$ $\bar{F}_{1/3}$	\bar{F}_{mean} $\bar{F}_{1/3}$
			\bar{x}	σ	σ/\bar{x}			
1/30	B1 ~ B10	0.367	0.153	0.081	0.529	1.88	1.25	0.752
		0.604	0.599	0.145	0.242	3.16	1.54	0.671
		0.676	0.808	0.172	0.213	3.38	1.51	0.640
	B3 (Run1~10)	0.676	0.834	0.164	0.197	3.39	1.67	0.504
1/100	B1 ~ B10	0.359	0.116	0.028	0.241	2.00	1.17	0.667
		0.549	0.425	0.199	0.468	3.91	1.45	0.636
		0.586	0.468	0.167	0.357	3.62	1.54	0.615
	B3 (Run1~10)	0.586	0.368	0.083	0.226	2.71	1.49	0.610

 \bar{x} : mean σ : standard deviation

of the breaking wave height is used to evaluate the breaking force parameter for irregular waves, and the maximum wave height in the figure is the maximum wave height in each wave group. Similar to the results in the regular wave tests, \hat{F} increases as the breaking parameter increases and the pile inclines seaward. However, the increasing curves are more straight in the figure than those for regular waves in Fig.10. That is, the wave force increases gradually with the increase of the breaking parameter. This is because various wave profiles can appear due to the combination of wave period and wave height in irregular waves.

6. CALCULATION METHOD

Outline of the Method

The calculation method is proposed in this chapter. The method is based on Karman's and Wagner's theories but is simplified considering the experimental results by regular and irregular waves. As shown in Fig. 15, the impact force is assumed to act on the pile with a triangular distribution. The peak value and the width of the distribution are denoted by f_p and δ . The height of the peak above the still water level is denoted by l_p . The distribution of the impact

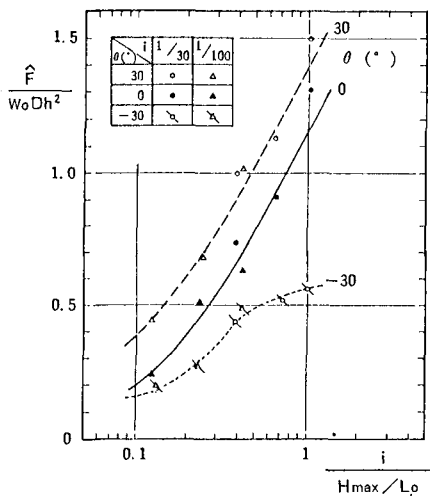


Fig.14 Maximum impact force

force is expressed by

$$f_z = \left\{ 1 - \frac{|l_p - z|}{\delta/2} \right\} f_p \quad \text{for } |l_p - z| < \delta/2 \quad (5)$$

where f_z is the impact force on the pile at the location z .

The impact force is also assumed to vary with respect to time t as a triangular pulse which has a vertical rise. The duration time is denoted by τ . Therefore, the time history of the impact force at the peak location is

$$f_p = f_{pm} \left(1 - \frac{t}{\tau} \right) \quad \text{for } 0 < t < \tau \quad (6)$$

where f_{pm} is the peak value of f_p with respect to time. The impact force at a certain point of the pile and at certain time is given by Eqs(5) and (6). The total impact force F_I and the peak value F_{Im} with respect to time in the calculation method are simply expressed by $0.5 \delta f_p$ and $0.5 \delta f_{pm}$ respectively.

Parameters

The parameters in the calculation method are determined as follows:

- a) Peak Value at Peak Location

The peak value at the peak location is assumed to be in the following form:

$$f_{pm} = \nu f_{km} \quad (7)$$

where f_{km} is the peak value which is obtained by Karman's theory and ν is the adjustment factor. Karman's peak value is expressed by

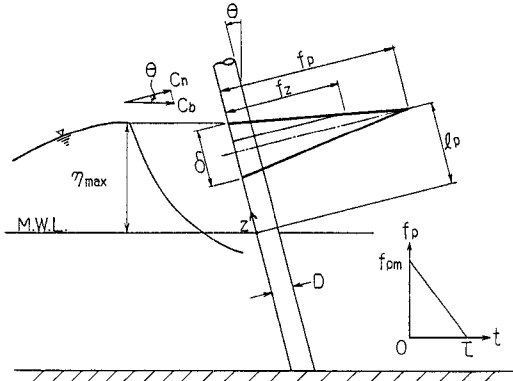


Fig.15 Impact force in the calculation method

$$f_{km} = \frac{\pi}{2g} w_0 C_n^2 D \quad (8)$$

where C_n is the wave celerity component perpendicular to the pile, which is

$$C_n = C_b \cos \theta \quad (9)$$

- b) Duration Time

According to Wagner's theory, the duration time and the impulse are about 0.4 and 0.65 times Karman's values respectively. The experimental results agree well with Wagner theory. Therefore, the duration time in the calculation method is assumed to be 0.5 times Karman's one as follows:

$$\tau = 0.25D/C_n \quad (10)$$

c) Height of the Peak Location above the Still Water Level

The height of the peak location above the still water level is averagedly 0.68 times the crest height for irregular waves in the experiments. Therefore, the height in the calculation method is assumed as

$$l_p = 0.75 \eta_b / \cos \theta \quad (11)$$

d) Distribution Width

The distribution width is averagedly 0.516 times the crest height for irregular waves in the experiments. The distribution width in the calculation method is approximated as

$$\delta = 0.5 \eta_b / \cos \theta \quad (12)$$

e) Adjustment Factor

The adjustment factor can be expressed by the following equation if the above relations are considered:

$$v = (8g \cos \theta / \pi^w_0 C_n^2 D) (F_{Im} / \eta_{max}) \quad (13)$$

The adjustment factor v was determined by the experimental data of F_{Im} with Eq.(13). It should be noted that the value of F_{Im} is the pure impact component which is subtracted the ordinary inertia and drag force component from the impact wave force. Two kinds of experimental values of F_{Im} were evaluated which were denoted by \bar{F}_I and \hat{F}_I . \bar{F}_I was evaluated by \bar{F}_{max} which is the average of F_{max} , and \hat{F}_I was evaluated by \hat{F} which is the maximum value of F_{max} in each wave group. Two kinds of the adjustment factors denoted by \bar{v} and \hat{v} are evaluated by \bar{F}_I and \hat{F}_I respectively. The adjustment factor in the calculation method was determined by these two adjustment factors as follows:

$$v = (0.8 + 0.4 \sin \theta) \tanh \left\{ 2.5 \log_{10} \frac{i / (H_{max} / L_0)}{0.25} \right\} + 1.0 + 1.2 \sin \theta \quad (14)$$

Comparison of Results

Figure 16 shows the comparison of the calculated value of the impact force by the above method with the experimental values. In the figure, both \bar{F}_I and \hat{F}_I are shown. The experimental values agree with the calculated values on the average, and the difference between them is regarded to be small if the tendency of the large variation in the impact force is taken into account.

The calculated value by the method can be compared with the

calculated value by the method in the Shore Protection Manual (1975). For example, when $h = 8 \text{ m}$, the wave height in deep water $H_0 = 6 \text{ m}$, $T_{1/3} = 10 \text{ s}$, $D = 1 \text{ m}$, and $i = 1/30$ and $1/100$, the maximum wave height H_{\max} can be obtained as 6.78 m for $i = 1/30$ and 6.06 m for $i = 1/100$ by Goda's diagram (see Goda (1985) pp. 71 - 87). The impact forces by the present method are 43.4 tf and 25 tf for $i = 1/30$ and $1/100$ respectively. These values are the pure impact component and the total impact forces become 55.4 tf and 47.3 tf if the ordinary inertia and drag component are evaluated to be 12.0 tf and 10.1 tf respectively. The impact breaking force by the method in Shore Protection Manual are nearly equal to the values by the present method for $i = 1/30$ but 35 % larger than the value by the method for $i = 1/100$.

7. CONCLUSIONS

- The major conclusions in the present study are as follows:
- 1) The peak values of the impact force on a circular pile by Wagner theory is larger than that by Karman's theory. The duration time and the impulse are about 0.4 and 0.65 times Karman's values respectively.
 - 2) As a pile inclined seaward, the impact force increase greatly. As the pile inclined shoreward, the impact force decreases. If the inclination angle is within 30° , the impact force varies 20 ~ 50 % compared with the force on the vertical pile.
 - 3) A new parameter called "the breaking force parameter", which is the ratio of bottom slope to wave steepness, can express the variation of the impact force. For regular waves, the impact force increases suddenly where the parameter is from 0.3 to 0.7. However, the impact force increases gradually with the increase of the parameter for irregular waves.
 - 4) A calculation method of the impact force is proposed. The method is based on Karman's and Wagner's theory, but is simplified considering the experimental results. The distribution shape of the impact force is approximated as a triangle. The impact force is also approximated as a triangular pulse with respect to time. The adjustment factor is introduced in the method which expresses the variation of the impact force due to the breaking parameter and the inclination angle. The calculated results by the method agree with the experimental results as a whole.

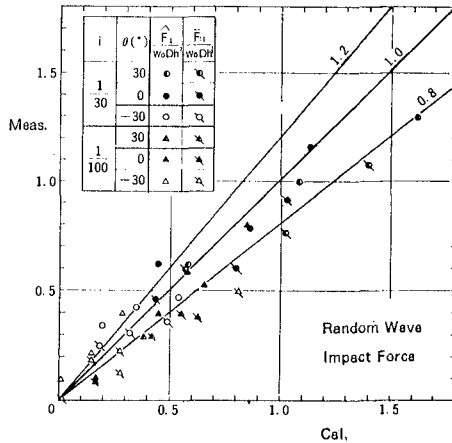


Fig.16 Comparison of the calculated results with experimental results

ACKNOWLEDGEMENT

The authors wish to thank Dr. Yoshimi Goda, Director General of the Port and Harbour Research Institute for his many precious comments during the course of this work.

REFERENCE

- Coastal Engineering Research Center (1975). Shore Protection Manual, U.S.Army Corps. of Engineers, Washington D.C., Vol.II.
- Goda, Y., Haranaka, S. and Kitahata, M.(1966) Study of impulsive breaking wave forces on piles, Rept. of Port and Harbour Res. Inst., Vol.5, No.6, pp.1-30 (in Japanese)
- Goda, Y. (1970). A synthesis of Breaker Indices, Trans, JSCE, Vol.2,pt 2, (in Japanese)
- Goda, Y. (1985). Random Seas and Design of Maritime Structures, Univ. of Tokyo Press, 323 p.
- Hall, M.A.(1958). Laboratory study of breaking wave force on piles, U.S. Army Corps of Engineers, Beach Erosion Board, Washington D.C., TM 106.
- Honda, J. and Mitsuyasu, H. (1974). Experimental Study of breaking wave force on a vertical circular cylinder, Coastal Engineering in Japan, Vol.17, pp.59-70.
- Ochi, M.K. and Tsai, C.H. (1984), Prediction of impact pressure induced by breaking waves on vertical cylinders in random seas, Applied Ocean Research, Vol.6, No.3, pp. 157-165.
- Ross, C.W. (1955). Laboratory study of shock pressures of breaking waves, U.S. Army Corps of Engineers, Beach Erosion Board, Washington D.C., TM 59.
- Ross, C.W.(1959). Large-scale tests of wave forces on piling, U.S. Army Corps of Engineers, Beach Erosion Board, Washington D.C., TM 111.
- Sawaragi, T. and Nochino, M. (1984) Impact forces of nearly breaking waves on a vertical circular cylinder, Coastal Engineering in Japan, Vol.27, pp.249-263.
- Tanimoto, K., Takahashi, S., Yoshimoto, Y.(1983). Estimation method of exciting shock force from a linear damped vibration system, Technical Note of the Port and Harbour Res. Inst., No.474, 24p. (in Japanese)
- Tanimoto, K., Takahashi, S., Kaneko, T. and Shiota, K. (1986A). Impulsive pressure of breaking wave on piles, Proc. 6th Offshore South East Asia, pp.492 -496.
- Tanimoto, K., Takahashi, S., Kaneko, T. and Shiota, K. (1986B), Impact force of breaking waves on an inclined pile, Proc. 5th Offshore Mechanics and Arctic Engineering Symposium., Vol.1, pp.235-241.
- Von Karman, Th. (1929). The impact on seaplane float during landing, NACA, TN321.
- Wagner, H. (1932) Über stoss-und gleitvorgänge an der oberfläche von flüssigkeiten, Zeitshrift für Angewandte Mathmatik und Mechanik, Band 12 Heft 4, pp.193-215.
- Watanabe, A. and Horikawa, K. (1974). Breaking wave forces on a large diameter cell, Proc. of 14th International Conference on Coastal Engineering, Chapter 102, pp.1741-1760.